energy&fuels

Article

Cite This: Energy Fuels 2018, 32, 11452−11466

pubs.acs.org/EF

Water Content and Equilibrium Saturation and Their Influencing Factors of the Lower Paleozoic Overmature Organic-Rich Shales in the Upper Yangtze Region of Southern China

Peng Cheng,[†] Xianming Xiao,*[,†,‡] Hui Tian,[†] and Xing Wang[†]

[†]State Key Laboratory of Organic Geochemistry, Guangzhou Institute of Geochemistry, Chinese Academy of Sciences, Guangzhou 510640, China

[‡]School of Energy Resources, China University of Geosciences, Beijing 100083, China

ABSTRACT: The geochemical and petrophysical characteristics of the Lower Paleozoic shales (the Lower Silurian Longmaxi Formation and the Lower Cambrian Niutitang Formation) in southern China have been well documented in recent years. However, the water content in these shales is less studied. Since water and hydrocarbons concomitantly distribute in the pore spaces of the shale reservoir, the water in the shale reservoir is important to the evaluation and development of its hydrocarbon resources. In the present study, the water content (C_{IW}) and equilibrium saturation (S_{EW}) of the two sets of overmature organic-rich shales, which were, respectively, collected from the Niutitang Formation of Fengye 1 well (FY1) and the Longmaxi Formation of Youqian 1 well (YQ1) in the Upper Yangtze Region of southern China, were investigated. The results show that the C_{IW} of the FY1 and YQ1 shales is 4.17−5.29 mg/g and 3.70−5.06 mg/g, respectively; the S_{EW} of the FY1 and YQ1 shales is 34.23−42.72% and 38.07−45.51%, respectively; and both sets of shales are in a subirreducible water-equilibrated state. The C_{IW} and C_{EIW} of these shales have positive correlations with their TOC content, total porosity, surface area, and pore volume of both the micropores and nonmicropores, but the S_{EW} has negative correlations with these parameters, indicating that the organic matter in these shales holds some water and that the TOC content mainly controls the C_{IW}, C_{EIW}, and S_{EW}. According to the regression lines in the TOC content vs C_{IW} plots and the TOC content vs C_{EIW} plots, the water equilibrium saturations of the organic-hosted pores (S_{OW}) and inorganic-hosted pores (S_{IW}) were estimated. The S_{IW} of these shales is greater than the S_{OW}, and the S_{IW}/S_{OW} ratio of the FY1 and YQ1 shales is 2.28 and 2.04, respectively, quantitatively indicating that the organic-hosted pores of these overmature shales are less hydrophilic than the inorganic-hosted pores. Therefore, for a set of overmature shales (FY1 or YQ1), with increasing TOC contents, the organic-hosted pore content increases and provides more storage space for the water in the shales, but the bulk hydrophilia of the shales reduces, leading to an increase in the C_{IW} and C_{EIW} and a decrease in the S_{EW}.

1. INTRODUCTION

The water content in a shale gas reservoir is important for evaluating its gas resources,[1,2] as it significantly influences both the free and absorbed shale gas content.[3,4] The Lower Silurian Longmaxi Formation and the Lower Cambrian Niutitang Formation organic-rich shales with equivalent vitrinite reflectance (EqRo) values of 2.5−4.5% developed widely in the Upper Yangtze Region of southern China.[5,6] The two sets of overmature shales are now the crucial strata for shale gas exploration in China[7−9] and have contributed more than 95% of shale gas production in China with an annual yield of shale gas of more than 90×10^8 m^3.[6,10,11] In recent years, the geochemical and petrophysical characteristics of the two sets of shales have been well documented.[12−16] Though undergoing intense dehydration during the diagenetic and thermal evolution stages,[17−19] the Lower Paleozoic overmature shales in southern China were generally found to contain connate water.[20,21] However, the water content in these shales is less studied, and the shale gas-producing areas in southern China generally lack the water content data, affecting the evaluation and prediction of shale gas potential in this area.[22,23]

The water content in shale strata is affected by several factors other than geological environments and thermal evolutions.[24−27] For example, the water content can be influenced by the content and composition of organic matter and inorganic minerals in shales due to their different water wettabilities[28−31] and by the porosity and pore structures of shales as they affect the interaction force between nanopore walls and water molecules.[32−34] In addition, the salinity of connate water, which influences the water adsorption and transport in the shale pore system,[35−37] may also have a certain effect on the water content in shales. At present, the factors affecting the water content of organic-rich shales are still not fully understood, especially for overmature shales, since the water wettability of organic and inorganic matter and the nanopore characteristics of these shales have been significantly transformed by thermal evolution.[24,38]

Shale gas reservoirs, especially with overmature shales, generally only contain irreducible water.[39] The methods of measuring water content in conventional reservoirs are generally invalid to shale reservoirs because of their very low permeability and porosity.[3,28,40−42] At present, the water content in shale gas reservoirs is mainly indirectly obtained from interpretations of well log data,[29] although such data obtained in this way are

Received: August 29, 2018
Revised: October 17, 2018
Published: October 18, 2018

DOI: 10.1021/acs.energyfuels.8b03011
Energy Fuels 2018, 32, 11452−11466

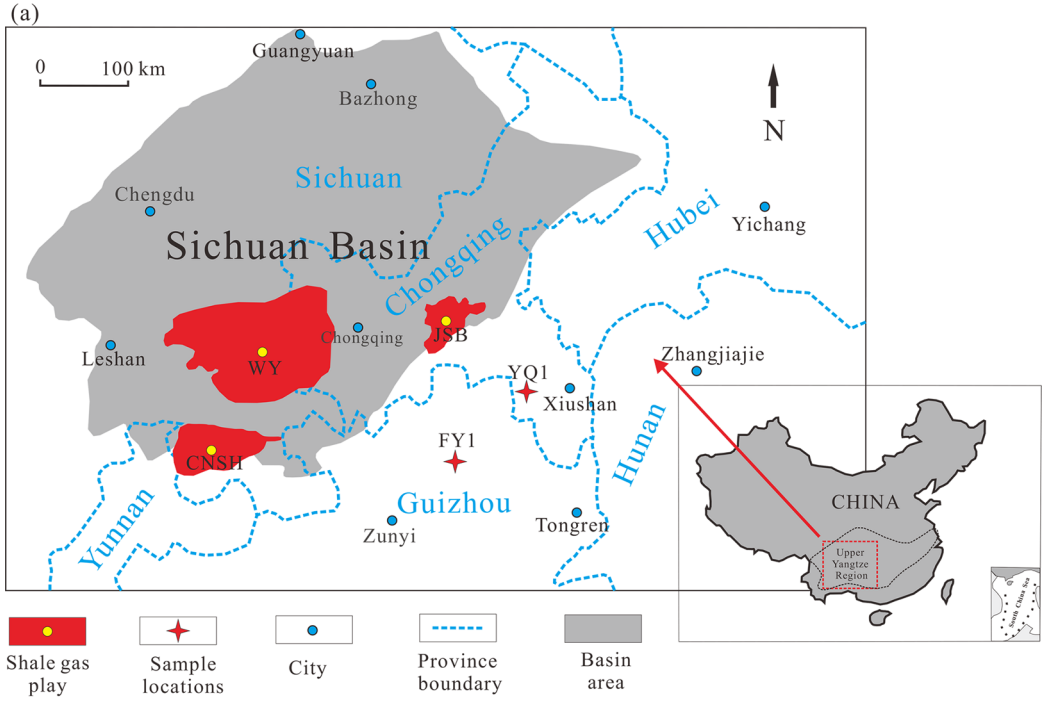

(b)

Strata				Lithology	Thickness (m)	Sedimentary facies
Erathem	System	Series	Formation			
Lower Paleozoic	Silurian	Lower	Shiniulan		200–500	Shallow water continental shelf
			Longmaxi		50–500	Deep water continental shelf
	Ordovician	Upper	Wufeng		3–10	
			Baota		14–55	Shallow water continental shelf
		Middle	Meitan		188–450	
		Lower	Honghuayuan		115–180	
	Cambrian	Upper	Xixiangchi		200–500	Semi-deep water continental shelf
		Middle	Douposi		0–200	
		Lower	Longwangmiao		150–660	
			Niutitang		150–350	Deep water continental shelf
Upper Proterozoic	Sinian	Upper	Dengying		330–1970	

Limestone Dolomite Silty mudstone Shale

Biolithite limestone Limy dolomite Siltstone Mudstone

Figure 1. Schematic maps showing the Upper Yangtze Region of southern China (a) and the stratigraphic column of this area (b). CNSH: Changning-Shuanghe; WY: Weiyuan; JSB: Jiaoshiba; FY1: Fengye 1 well; YQ1: Youqian 1 well (modified with permission from ref 6).

usually inaccurate due to the low porosity and permeability of organic-rich shales.[43−45] Because it is difficult to obtain typical shale samples with preserved water characteristics in geological conditions, as-received shale or coal samples are commonly used in laboratory studies.[42,46−48] It was reported that the water characteristics of as-received shale samples undergo approx-

DOI: 10.1021/acs.energyfuels.8b03011
Energy Fuels 2018, 32, 11452−11466

Table 1. Conventional Geochemical Characteristics and Mineral Compositions of the FY1 and YQ1 Shales

sample information							mineral compositions (%)[a]					
									clays			
well	stratum	number	depth (m)	lithology	TOC (%)[a]	BRo (%)[b]	quartz	feldspar	illite	chlorite	carbonate	others
FY1	Lower Cambrian	FY1-1	2448.54	black shale	1.76	——[c]	29.3	28.4	33.3	0.0	6.5	2.4
		FY1-2	2449.44		2.70	3.95	31.6	32.1	28.5	0.0	5.4	2.3
		FY1-3	2450.8		3.67	——	33.6	36.9	17.7	0.0	6.5	5.3
		FY1-4	2455.85		4.51	3.82	31.4	33.0	25.0	0.0	6.4	4.2
		FY1-5	2457.3		6.38	——	39.3	26.9	23.7	0.0	5.9	4.2
		FY1-6	2458.4		5.42	4.06	33.7	29.0	26.2	0.0	6.1	5.0
		FY1-7	2480.95		7.85	——	39.1	30.6	21.9	0.0	5.2	3.3
		FY1-8	2496.79		7.59	4.13	27.4	44.1	21.6	0.0	0.0	6.8
		FY1-9	2533		8.68	——	68.0	8.9	18.0	0.0	3.1	2.0
YQ1	Lower Silurian	YQ1-1	1123.87	black shale	1.63	——	31.5	22.8	22.4	17.1	5.3	0.9
		YQ1-2	1126.71		1.94	2.73	27.8	22.9	25.3	15.1	7.0	1.9
		YQ1-3	1129.27		2.48	——	35.3	19.9	27.5	8.7	6.0	2.5
		YQ1-4	1136.02		2.94	——	29.5	19.0	24.2	11.8	13.8	1.7
		YQ1-5	1143.36		3.19	3.05	38.9	13.3	30.3	8.1	7.5	1.8
		YQ1-6	1145.90		3.64	——	33.2	19.8	21.6	11.4	10.4	3.5
		YQ1-7	1147.70		4.08	——	50.7	5.5	21.0	11.6	9.4	1.9
		YQ1-8	1149.35		4.59	2.96	33.2	14.7	28.4	11.0	9.2	3.5
		YQ1-9	1161.76		5.03	——	43.8	14.3	24.6	10.0	2.9	4.4

[a]Data cited from ref 49. [b]Mean pyrobitumen reflectance. [c]No data.

imately no significant changes for two years when sealed in Ziploc bags and preserved at an ambient temperature because of their low permeability and porosity and abundant nanopores.[3] Therefore, as-received shale samples were commonly used in studying the water characteristics of shales. In a previous study, the equilibrium irreducible water contents (C_{EIW}, the water content in moisture-equilibrated shale samples at a relative humidity of 96−97% and 30 °C) of two sets of as-received overmature organic-rich shale samples, which were derived from the Niutitang Formation of the Fengye 1 well (FY1) and the Longmaxi Formation of the Youqian 1 well (YQ1) in the Upper Yangtze Region of southern China, were investigated by a water adsorption experiment.[49] In the present study, the water content (C_{IW}) and equilibrium saturation (S_{EW}, the percentage of C_{IW} in C_{EIW}) of the two sets of typical overmature shales, which were used to, respectively, characterize the irreducible water content in as-received shale samples and the degree of the irreducible water in these shales reaching moisture equilibrium, were further investigated. Combining with the organic and inorganic compositions and the pore characteristics of these two sets of shale samples, the factors influencing the C_{IW}, C_{EIW}, and S_{EW} of these overmature shales are also discussed. The present study is to provide a further understanding on water distribution in the pore system of shales and to determine the main controlling factor of the water content in these overmature shales.

2. SAMPLES AND EXPERIMENTS

2.1. Sample Information. In the present study, shale samples were derived from the Fengye 1 (FY1) and Youqian 1 (YQ1) test wells in the Upper Yangtze Region of southern China (Figure 1a), and their target formations are the Niutitang Formation of the Lower Cambrian and the Longmaxi Formation of the Lower Silurian, respectively (Figure 1b). A shale core sample was broken into large pieces when taken out of the test well, and the large pieces originally located in the inner part of the shale core were selected and sealed in Ziploc bags for laboratory studies since the external part of that may be polluted by the imbibition of drilling fluids. The selected large pieces of shale cores generally contain some gases (they bubble when immersed in water), which prevents external water from accessing them during the drilling process. Therefore, the water content in these shale pieces is believed to be slightly influenced during the drilling process and to approximately represent their connate water content.[3] However, it should be pointed out that the risk could not be totally eliminated.

The conventional geochemical characteristics and mineral compositions of these shale samples were reported in a previous study[49] and are briefly summarized here (Table 1). The FY1 samples have a TOC content of 1.76−8.68%, and their quartz, feldspar, and clay minerals are 27.4−68%, 8.9−44.1%, and 17.7−33.3%, respectively. The YQ1 samples have a TOC content of 1.63−5.03%, and their quartz, feldspar, and clay minerals are 27.8−50.7%, 5.5−22.9%, and 32.6−40.4%, respectively. The measured pyrobitumen reflectance values are 3.82−4.13% for the FY1 shales and 2.73−3.05% for the YQ1 shales, respectively, corresponding to 3.87−4.17% and 2.83−3.14% equivalent vitrinite reflectance values (ER_O) according to Schoenherr et al.[50]

2.2. Experiments. *2.2.1. Measurement of the C_{IW} and S_{EW} of Shales.* Small cylindrical cores with a diameter of 15 mm and a length of 20 mm were drilled from the selected shale core samples to measure their C_{IW} in the present study. The small shale core samples were first weighed to obtain their as-received mass (m_{AR}, g). Then, they were loaded into a vacuum oven (<30 mmHg), and their dry mass (m_{Dry}, g) was obtained by holding at 105 °C for 12 h in the oven. The water content (C_{IW}, mg/g) of a shale sample can be calculated by eq 1:

$$C_{IW} = [(m_{AR} - m_{Dry}) \times 1000]/m_{Dry} \quad (1)$$

Combined with the equilibrium irreducible water contents (C_{EIW}, mg/g) reported by a previous study[49] (see Table 2), the water equilibrium saturations (S_{EW}, %) of these shale samples can be further calculated by eq 2:

$$S_{EW} = C_{IW}/C_{EIW} \times 100 \quad (2)$$

The water equilibrium saturation (S_{EW}) rather than the conventional water saturation (the percentage of water volume in total pore volume) is used in the present study because the average density of the irreducible water, which was used in calculation of its volume, differs from that of its bulk phase, significantly changes with pore types (organic-hosted or inorganic-hosted pores) and pore sizes (micropores or nonmicropores),[51] and varies with the thickness in nanopore walls.[52] Compared to the conventional water saturation, the S_{EW} is a more

DOI: 10.1021/acs.energyfuels.8b03011
Energy Fuels 2018, 32, 11452−11466

Table 2. Water Content (C_{IW}) and Equilibrium Irreducible Water Content (C_{EIW}) as Well as the Water Equilibrium Saturation (S_{EW}) of the FY1 and YQ1 Samples

sample information[a]		water content (mg/g)	equilibrium irreducible water content (mg/g)[b]	water equilibrium saturation (%)[c]
well	number			
FY1	FY1-1	4.17	9.77	42.72
	FY1-2	4.37	10.40	42.02
	FY1-3	4.39	11.76	37.35
	FY1-4	4.68	12.66	36.98
	FY1-5	5.04	14.06	35.83
	FY1-6	4.73	13.49	35.08
	FY1-7	5.09	14.87	34.23
	FY1-8	5.15	14.94	34.44
	FY1-9	5.29	15.04	35.18
YQ1	YQ1-1	3.70	8.13	45.45
	YQ1-2	3.78	8.30	45.51
	YQ1-3	4.03	10.04	40.13
	YQ1-4	4.79	11.24	42.60
	YQ1-5	4.28	10.98	38.97
	YQ1-6	4.56	11.80	38.65
	YQ1-7	5.06	12.65	40.02
	YQ1-8	4.72	12.41	38.07
	YQ1-9	4.78	12.48	38.30

[a]Sample information, see Table 1. [b]Data cited from ref 49. These data were obtained at an equalized moisture condition with a relative humidity of 96–97% and 30 °C. [c]The percentage of water content (C_{IW}) in equilibrium irreducible water content (C_{EIW}).

suitable parameter to discuss the factors influencing the water in overmature shales as only irreducible water is present in them.[39]

2.2.2. Analysis of Total Porosity. In the present study, the total porosity of a shale sample was determined by its skeletal and bulk density as described by Chalmers et al.[53] The skeletal (ρ_s, g/cm^3) and bulk densities (ρ_B, g/cm^3) of a dried cylindrical shale core sample were, respectively, measured by a helium pycnometry instrument (the Quantachrome Ultra-Pore 300) at an ambient temperature (25 °C) and a hydrometer (DH-1200M, Daho Meter) according to the sealing paraffin method.[12] The total porosity (Φ, %) can be calculated using eq 3:

$$\Phi = (1 - \rho_B/\rho_S) \times 100 \quad (3)$$

2.2.3. Analysis of Pore Structures. Shale nanopores are generally divided into micropores (<2 nm), mesopores (2–50 nm). and macropores (>50 nm) based on the IUPAC standards (International Union of Pure and Applied Chemistry).[54] In the present study, the low-pressure CO_2 and N_2 adsorption experiments which performed on a Micromeritics ASAP 2020 M apparatus were used to characterize the micropore and nonmicropore (including mesopores and macropores) structures of shales, respectively. The low-pressure gas adsorption experiments were commonly used,[12,13,15,53,55−58] and the main procedures are briefly summarized below. The small cylindrical shale core sample was first dried at 105 °C for 6 h and was gently crushed into 20–40 mesh (380–830 μm) in a stainless steel mortar. Then, these shale grains were loaded into the testing apparatus, which was evacuated to a high vacuum of approximately 10 mmHg, and were degassed at 110 °C for 12 h. The samples were tested at −196.56 °C (liquid nitrogen environment) and a relative pressure of 0.005–0.995 for the N_2 adsorption and at 0 °C (ice–water mixture environment) and a relative pressure of 0.00001 to 0.032 for the CO_2 adsorption. The Dubinin–Astakhov equation was used to calculate the volume (V_{mic}) and surface area (S_{mic}) of micropore according to the CO_2 adsorption data.[59] The modified Brunauer–Emmett–Teller equation was used to calculate the surface area ($S_{n\text{-}mic}$) of nonmicropore based on the N_2 adsorption data.[13,60] The maximum adsorption value in the N_2 adsorption isotherm multiplied by the density conversion factor of 0.001547 gave the total volume, and the total volume subtracting the micropore volume gave the nonmicropore volume ($V_{n\text{-}mic}$).[13,15,58]

3. RESULTS AND DISCUSSION

3.1. C_{IW} and S_{EW} of Shales and Their Relationships with TOC and Clay Mineral Contents. The C_{IW} of the FY1 and YQ1samples is 4.17–5.29 mg/g and 3.70–5.06 mg/g, respectively, and the average C_{IW} of the FY1 and YQ1 samples is 4.77 mg/g and 4.41 mg/g, respectively (Table 2). The C_{IW} of the two sets of shales are considerably lower than their C_{EIW}, indicating only irreducible water in these overmature shales. The S_{EW} is 34.23–42.72% with an average of 37.09% for the FY1 samples and is 38.07–45.51% with an average of 40.86% for the YQ1 samples (Table 2), indicating these shale samples have not been equilibrated by the irreducible water. Comparing with the YQ1 shales, the FY1 shales have slightly higher C_{IW} values and slightly lower S_{EW} values (Table 2). Additionally, the C_{IW} of these shale samples is positively correlated with the C_{EIW} and is negatively correlated with the S_{EW} (Figure 2), indicating that, for a set of overmature organic-rich shales (FY1 or YQ1), the shales with a higher C_{IW} may have a higher C_{EIW} and a lower S_{EW}.

The TOC contents of the two sets of shales clearly have positive correlations with the C_{IW}, with a coefficient (R^2) of 0.97 and 0.72 for the FY1 and YQ1 shales, respectively (Figure 3a), and have negative correlations with the S_{EW}, with a coefficient

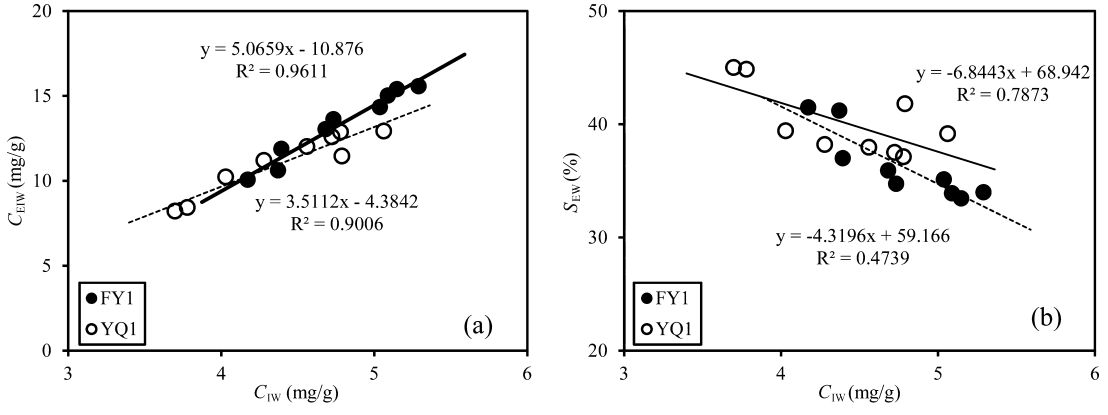

Figure 2. Correlations of water content (C_{IW}) with equilibrium irreducible water content (C_{EIW}) (a) as well as water equilibrium saturation (S_{EW}) (b) of the studied shale samples. The C_{EIW} data of shale samples are cited from ref 49.

DOI: 10.1021/acs.energyfuels.8b03011
Energy Fuels 2018, 32, 11452−11466

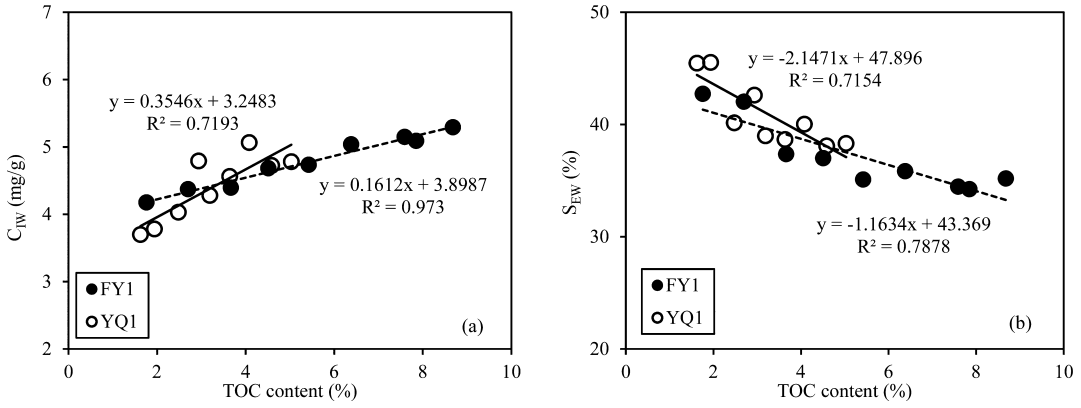

Figure 3. Correlations of the TOC content with the water content (C_{IW}) (a) and equilibrium saturation (S_{EW}) (b) of the studied shale samples.

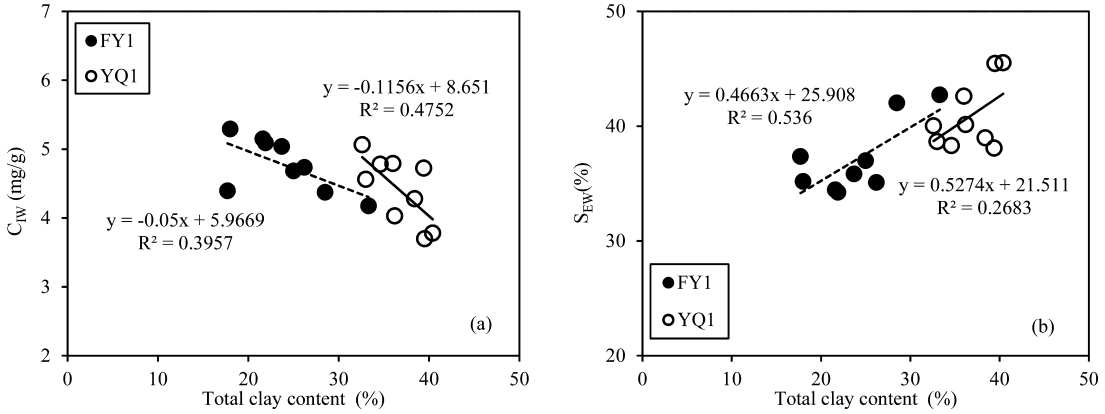

Figure 4. Correlations of the total clay mineral content with the water content (C_{IW}) (a) and equilibrium saturation (S_{EW}) (b) of the studied shale samples.

Table 3. Total Porosity, Pore Volume, and Surface Area of the FY1 and YQ1 Samples

sample information[a]			micropore		nonmicropore[b]		total pore	
well	number	total porosity (%)	pore volume (cm^3/g)	surface area (m^2/g)	pore volume (cm^3/g)	surface area (m^2/g)	pore volume (cm^3/g)	surface area (m^2/g)
FY1	FY1-1	1.43	0.0042	10.58	0.0041	3.86	0.0083	14.43
	FY1-2	1.51	0.0041	10.25	0.0046	4.13	0.0087	14.38
	FY1-3	1.55	0.0053	13.21	0.0056	5.43	0.0109	18.65
	FY1-4	2.10	0.0059	14.72	0.0052	5.79	0.0111	20.51
	FY1-5	2.23	0.0058	14.58	0.0069	6.58	0.0128	21.16
	FY1-6	2.23	0.0068	16.90	0.0059	7.06	0.0126	23.96
	FY1-7	3.02	0.0071	17.66	0.0057	7.96	0.0128	25.62
	FY1-8	3.17	0.0061	15.15	0.0065	7.12	0.0126	22.27
	FY1-9	3.57	0.0072	18.07	0.0066	8.20	0.0138	26.28
YQ1	YQ1-1	1.83	0.0034	8.54	0.0054	3.41	0.0088	11.95
	YQ1-2	1.86	0.0034	8.56	0.0063	4.09	0.0097	12.65
	YQ1-3	2.53	0.0044	11.00	0.0067	4.89	0.0112	15.89
	YQ1-4	2.77	0.0049	12.30	0.0068	5.19	0.0117	17.48
	YQ1-5	2.94	0.0050	12.52	0.0073	5.80	0.0123	18.31
	YQ1-6	2.76	0.0056	14.05	0.0074	5.77	0.0131	19.82
	YQ1-7	3.53	0.0062	15.56	0.0073	6.08	0.0136	21.64
	YQ1-8	3.18	0.0058	14.36	0.0074	5.79	0.0132	20.16
	YQ1-9	3.30	0.0075	18.73	0.0075	6.92	0.0150	25.65

[a]For sample information, see Table 1. [b]Nonmicropore includes mesopore and macropore.

(R^2) of 0.79 and 0.72 for the FY1 and YQ1 shales, respectively (Figure 3b). However, the total clay mineral contents of the two sets of shales have weakly negative correlations with the C_{IW} (Figure 4a) and have weakly positive correlations with the S_{EW} (Figure 4b). The similar correlations of the TOC content and total clay mineral content with the C_{EIW} of the two sets of shales were also observed in a previous study.[49] Since the TOC contents of the two sets of shales also have negative correlations

DOI: 10.1021/acs.energyfuels.8b03011
Energy Fuels 2018, 32, 11452−11466

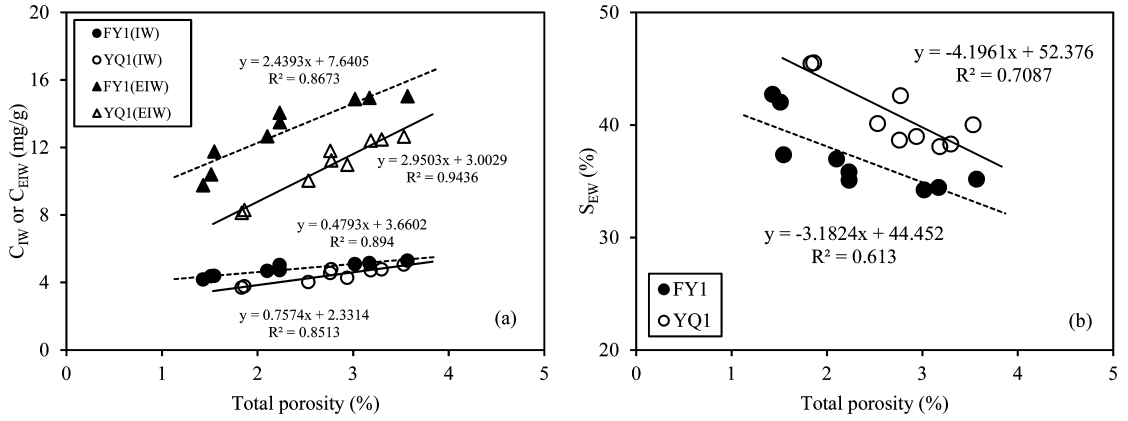

Figure 5. Correlations of total porosity with water content (C_{IW}) and equilibrium irreducible water content (C_{EIW}) (a) as well as water equilibrium saturation (S_{EW}) (b) of the studied shales samples. The C_{EIW} data of shale samples are cited from ref 49.

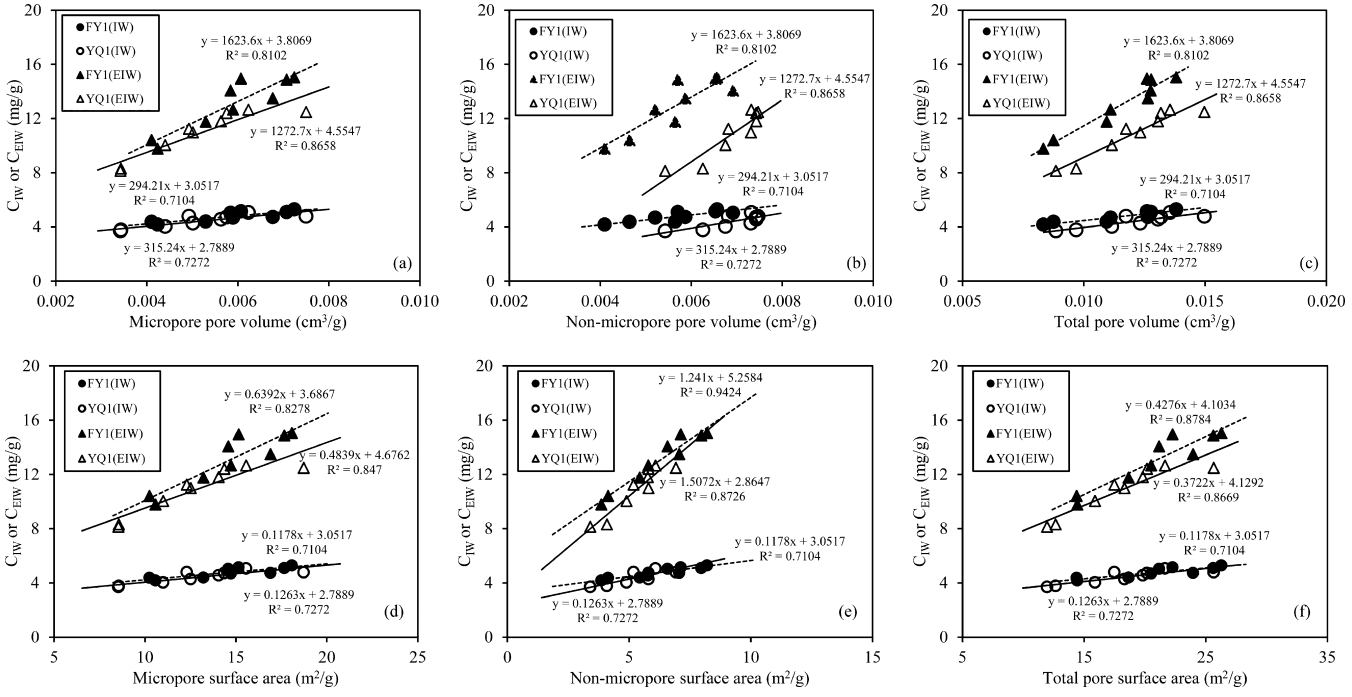

Figure 6. Correlations of the water content (C_{IW}) and equilibrium irreducible water content (C_{EIW}) with the pore volume and surface area of the micropores (a, d), nonmicropores (b, e), and total pores (c, f) of the studied shale samples. The C_{EIW} data of shale samples are cited from ref 49.

with the total clay minerals,[49] the C_{IW} and S_{EW} of the two sets of overmature shales are mainly controlled by their TOC contents compared with their total clay mineral content. Though the quartz and feldspar relative contents of the two sets shales are high (Table 1), they have no significant effects on the C_{IW} and S_{EW} because few pores developed in these brittle minerals.

3.2. Porosity and Pore Structures of Shales and Their Relationships with the C_{IW}, C_{EIW}, and S_{EW}.

The total porosity is 1.43−3.57% with an average of 2.31% for the FY1 the samples and is 1.83−3.53% with an average of 2.75% for the YQ1 samples (Table 3). The total porosity of both sets of shales has a positive correlation with the C_{IW} and C_{EIW}, with coefficients (R^2) of 0.89 and 0.87 for the FY1 samples and with coefficients (R^2) of 0.85 and 0.94 for the YQ1 samples (Figure 5a). However, the total porosity of these shales shows a negative correlation with the S_{EW}, with a coefficient (R^2) of 0.61 for the FY1 samples and with a coefficient (R^2) of 0.71 for the YQ1 samples (Figure 5b).

Table 3 shows the pore structure parameters of the FY1 and YQ1 shales. The micropore, nonmicropore (mesopore + macropore), and total pore (micropore + nonmicropore) volumes of the FY1 shales are 0.0041−0.0072 cm^3/g, 0.0041−0.0069 cm^3/g, and 0.0083−0.0138 cm^3/g, respectively; the micropore, nonmicropore, and total surface areas of this set of shales are 10.25−18.07 m^2/g, 3.86−8.20 m^2/g, and 14.38−26.28 m^2/g, respectively. The micropore, nonmicropore, and total pore volumes of the YQ1 shales are 0.0034−0.0075 cm^3/g, 0.0054−0.0075 cm^3/g, and 0.0088−0.0150 cm^3/g, respectively; the micropore, nonmicropore, and total surface areas of this set of shales are 8.54−18.73 m^2/g, 3.41−6.92 m^2/g, and 11.95−25.65 m^2/g, respectively. The above pore structure parameters of these shales have positive correlations with the C_{IW} and C_{EIW}, with coefficients (R^2) of 0.71−0.73 and 0.81−0.94, respectively (Figure 6), and have negative relationships with the S_{EW}, with coefficients (R^2) of 0.66−0.92 (Figure 7). It was noted that there is an obvious difference in the regression line slopes between the

DOI: 10.1021/acs.energyfuels.8b03011
Energy Fuels 2018, 32, 11452−11466

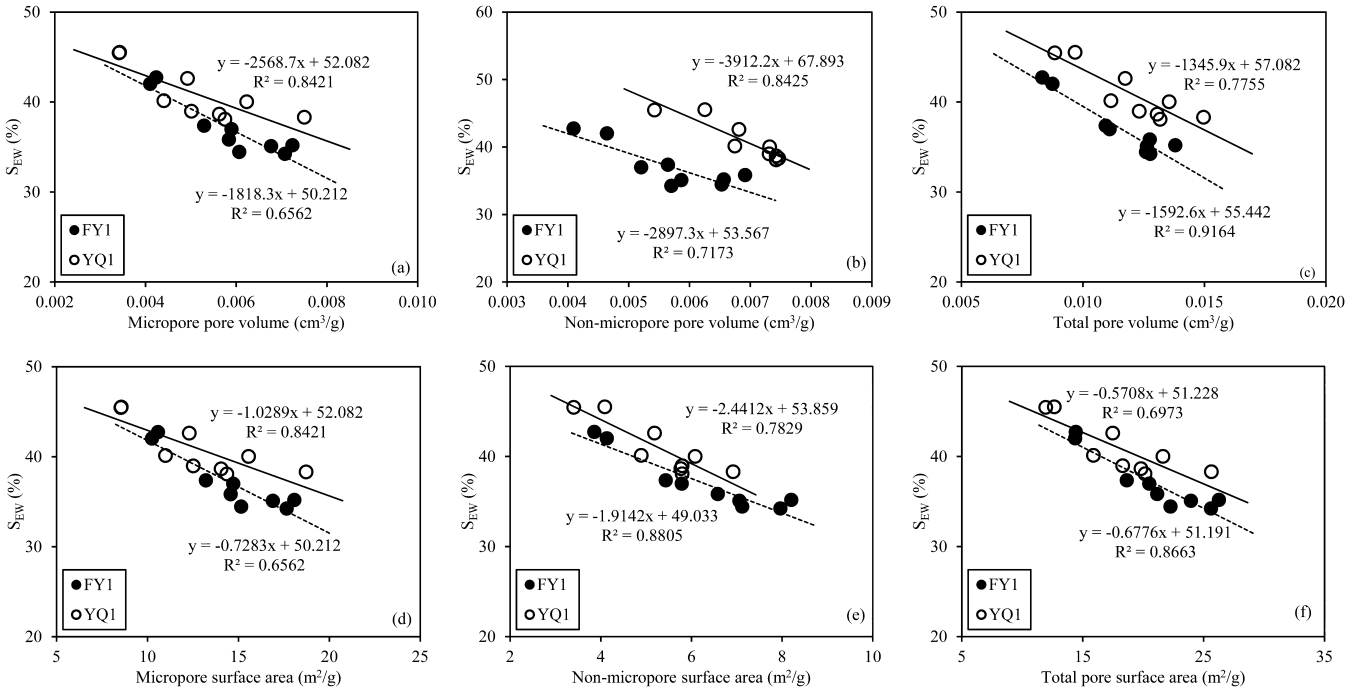

Figure 7. Correlations of the water equilibrium saturation (S_{EW}) with the pore volume and surface area of the micropores (a, d), nonmicropores (b, e), and total pores (c, f) of the studied shale samples.

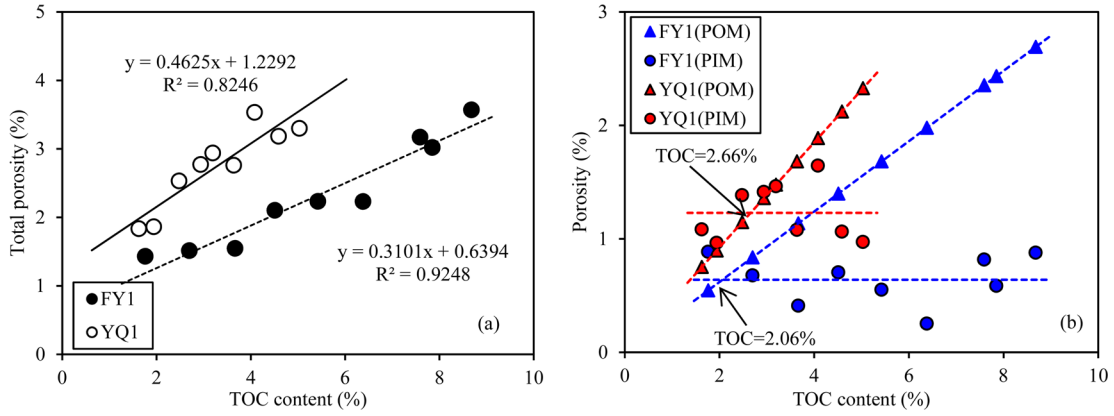

Figure 8. Correlations of the TOC content with the total (a), organic-hosted (P_{OM}), and inorganic-hosted (P_{IM}) porosity (b) of the studied shale samples.

C_{EIW} vs S_{mic} (Figure 6d) and the C_{EIW} vs $S_{n\text{-}mic}$ (Figure 6e), which implies that the nonmicropore surface area may have a stronger effect on the irreducible water than the micropore surface area at the moisture-equilibrated state.[49]

According to the above results, the water in the studied overmature shale samples occurs widely in both micropores and nonmicropores, and the C_{IW}, C_{EIW}, and S_{EW} are obviously constrained by the porosity and pore structure parameters.

3.3. Organic-Hosted and Inorganic-Hosted Pores.

Since the organic matter and inorganic minerals of shales have different water wettabilities,[28−31,42] the organic-hosted and inorganic-hosted pores would be different in capacity of holding water and then affect the C_{IW}, C_{EIW}, and S_{EW}. Therefore, the organic-hosted and inorganic-hosted pores of these shales were characterized in the studied samples.

The TOC contents of both the FY1 and YQ1 samples show remarkable linear positive correlations with the total porosity, and the coefficient (R^2) is 0.92 for the FY1 shales and 0.82 for the YQ1 shales (Figure 8a). The slope of the regression line in the TOC content vs total porosity plot (Figure 8a) represents the average organic-hosted porosity of per 1% of TOC content (W_{OM}).[12,13] Then, the organic-hosted porosity (P_{OM}) of these shales can be estimated based on the W_{OM} and their TOC content (TOC × W_{OM}), and the inorganic-hosted porosity (P_{IM}) can be obtained by subtracting the P_{OM} from the total porosity of these shales. The results show that the P_{OM} of the FY1 and YQ1 shales are 0.55−2.69% and 0.75−2.33%, respectively, and that the P_{IM} of the FY1 and YQ1 shales are 0.25−0.88% and 0.96−1.64%, respectively (Table 4). For a given TOC content, the P_{OM} and P_{IM} of the YQ1 samples (with a lower maturity) are higher than those of the FY1 samples (with a higher maturity) (Figure 8b). Additionally, with increasing TOC contents, in both sets of shales, the P_{IM} shows no apparent changes, but the P_{OM} significantly increases; the P_{OM} is greater than the P_{IM} when the TOC content of the FY1 and YQ1 shales is larger than 2.06% and 2.66%, respectively (Figure 8b).

DOI: 10.1021/acs.energyfuels.8b03011
Energy Fuels 2018, 32, 11452−11466

Table 4. Organic-Hosted and Inorganic-Hosted Porosity, Micropore Volume, and Nonmicropore Surface Area of the FY1 and YQ1 Samples

sample information[a]		total porosity[b]			micropore volume			nonmicropore surface area		
well	number	P_{OM} (%)	P_{IM} (%)	P_{IM}/P_{OM}	$V_{OM\text{-}mic}$ (cm^3/g)	$V_{IM\text{-}mic}$ (cm^3/g)	$V_{IM\text{-}mic}/V_{OM\text{-}mic}$	$S_{OM\text{-}non}$ (m^2/g)	$S_{IM\text{-}non}$ (m^2/g)	$S_{IM\text{-}non}/S_{OM\text{-}non}$
FY1	FY1-1	0.55	0.88	1.62	0.0007	0.0035	5.02	1.09	2.76	2.53
	FY1-2	0.84	0.68	0.81	0.0011	0.0030	2.80	1.68	2.46	1.47
	FY1-3	1.14	0.41	0.36	0.0015	0.0038	2.61	2.28	3.16	1.39
	FY1-4	1.40	0.70	0.50	0.0018	0.0041	2.27	2.80	2.99	1.07
	FY1-5	1.98	0.25	0.13	0.0026	0.0033	1.29	3.96	2.62	0.66
	FY1-6	1.68	0.55	0.33	0.0022	0.0046	2.12	3.37	3.69	1.10
	FY1-7	2.43	0.58	0.24	0.0031	0.0039	1.25	4.87	3.09	0.63
	FY1-8	2.35	0.82	0.35	0.0030	0.0030	1.00	4.71	2.41	0.51
	FY1-9	2.69	0.88	0.33	0.0035	0.0038	1.09	5.39	2.81	0.52
YQ1	YQ1-1	0.75	1.08	1.44	0.0018	0.0016	0.91	1.40	2.00	1.43
	YQ1-2	0.90	0.96	1.07	0.0021	0.0013	0.61	1.67	2.41	1.44
	YQ1-3	1.15	1.38	1.21	0.0027	0.0017	0.61	2.14	2.75	1.29
	YQ1-4	1.36	1.41	1.04	0.0032	0.0017	0.52	2.54	2.65	1.05
	YQ1-5	1.48	1.46	0.99	0.0035	0.0015	0.43	2.76	3.04	1.10
	YQ1-6	1.68	1.08	0.64	0.0040	0.0016	0.41	3.14	2.63	0.84
	YQ1-7	1.89	1.64	0.87	0.0045	0.0017	0.39	3.52	2.56	0.73
	YQ1-8	2.12	1.06	0.50	0.0050	0.0007	0.14	3.96	1.84	0.46
	YQ1-9	2.33	0.97	0.42	0.0055	0.0020	0.36	4.34	2.58	0.59

[a]For sample information, see Table 1. [b]P_{OM} and P_{IM}: the organic-hosted and inorganic-hosted porosity; $V_{OM\text{-}mic}$ and $V_{IM\text{-}mic}$: the organic-hosted and inorganic-hosted micropore volume; $S_{OM\text{-}non}$ and $S_{IM\text{-}non}$: the organic-hosted and inorganic-hosted nonmicropore surface area.

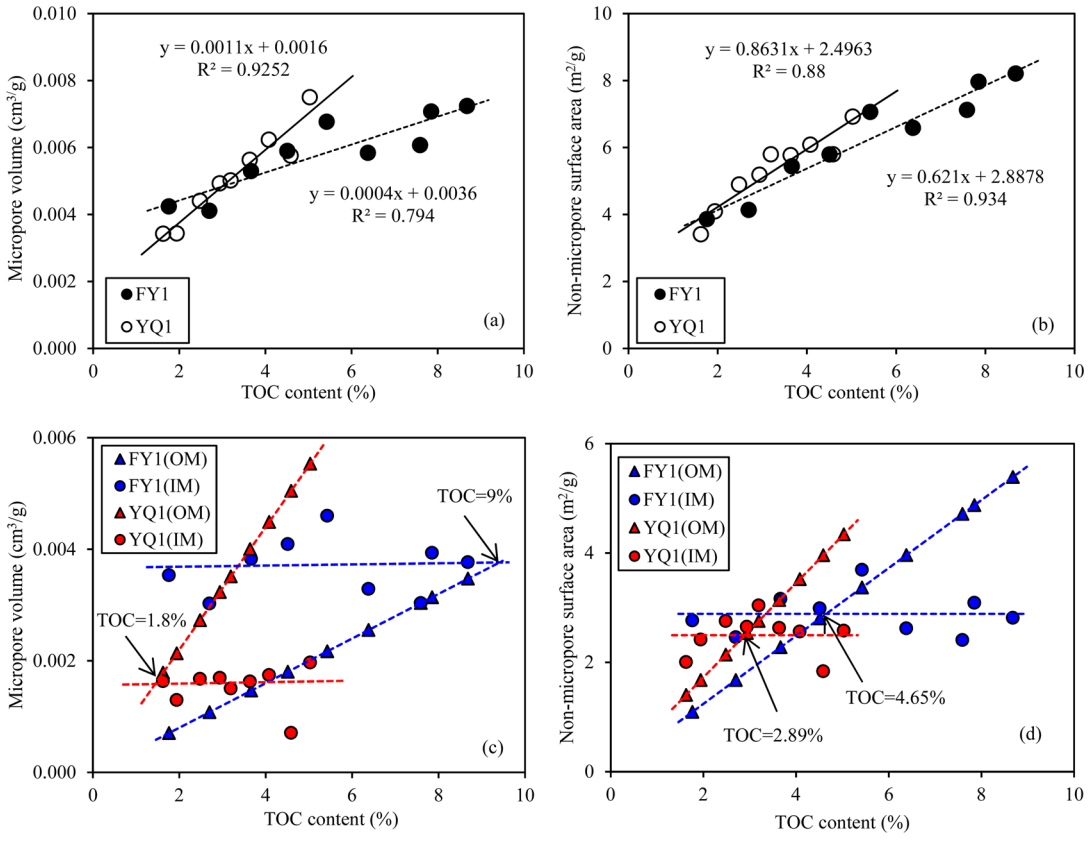

Figure 9. Correlations of the TOC content with the total micropore volume (a), total nonmicropore surface area (b), the organic-hosted and inorganic-hosted micropore volume (c), and the organic-hosted and inorganic-hosted nonmicropore surface area (d) of the studied shale samples.

It was reported that irreducible water has different distributions and occurrences in micropores and nonmicropores of shales. The irreducible water is either condensed in the micropores, mainly controlled by the volume and water wettability of the micropores, or absorbed in the nonmicropores, mainly controlled by the surface area and water wettability of the nonmicropores.[33,49,61,62] Therefore, shale micropore volume and nonmicropore surface area, as well as the water wettability of

DOI: 10.1021/acs.energyfuels.8b03011
Energy Fuels 2018, 32, 11452−11466

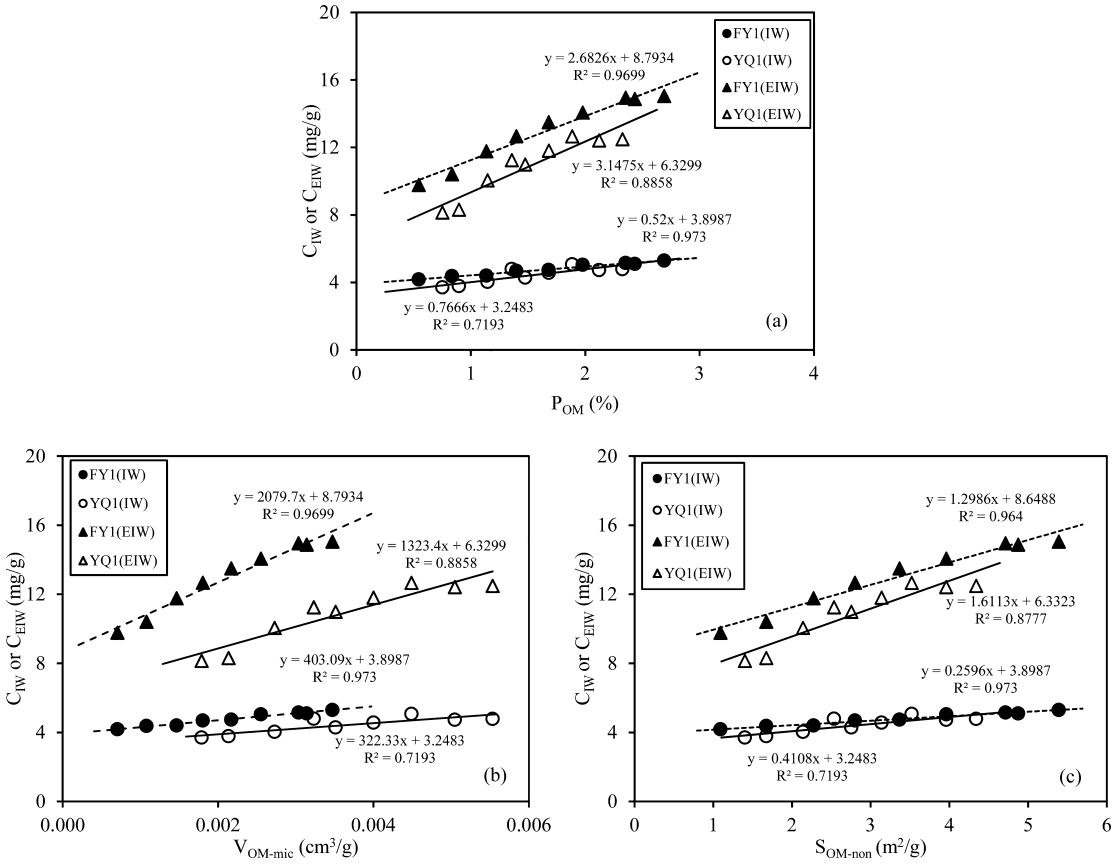

Figure 10. Correlations of the water content (C_{IW}) and equilibrium irreducible water content (C_{EIW}) with the organic-hosted porosity (P_{OM}) (a), organic-hosted micropore volume ($V_{OM\text{-}mic}$) (b), and organic-hosted nonmicropore surface area ($S_{OM\text{-}non}$) (c) of the studied shale samples. The C_{EIW} data of shale samples are cited from ref 49.

the two different sized pores, have remarkable influences on the C_{IW}, C_{EIW}, and S_{EW}. The TOC contents of the FY1 and YQ1 samples clearly have remarkable linear positive correlations with the micropore volume, and the coefficient (R^2) is 0.79 for the FY1 shales and 0.93 for the YQ1 shales (Figure 9a). The TOC contents clearly have remarkable linear positive correlations with the nonmicropore surface area, and the coefficient (R^2) is 0.93 for the FY1 shales and 0.88 for the YQ1 shales (Figure 9b). Therefore, based on the slopes of the regression lines in Figure 9a and b and the TOC contents of these shales, the organic-hosted and inorganic-hosted pore structure parameters of these shales were also obtained by the above-mentioned method (Table 4, Figure 9c and d).

For a given TOC content, the micropore volume and nonmicropore surface area of the YQ1 samples are larger than these of the FY1 samples (Figure 9a,b). With increasing TOC contents, the inorganic-hosted pore structure parameters of the FY1 and YQ1 samples show no significant changes, but the organic-hosted pore structure parameters of these shales significantly increase and lead to an increase in the total pore structure parameters (Table 4 and Figure 9c and d). The organic-hosted ($V_{OM\text{-}mic}$) and inorganic-hosted ($V_{IM\text{-}mic}$) micropore volumes of the FY1 samples are 0.0007−0.0035 cm^3/g and 0.0030−0.0046 cm^3/g, respectively, and the $V_{OM\text{-}mic}$ of this set of shale samples is smaller than its $V_{IM\text{-}mic}$. The organic-hosted ($S_{OM\text{-}non}$) and inorganic-hosted ($S_{IM\text{-}non}$) nonmicropore surface areas of the FY1 samples are 1.09−5.39 m^2/g and 2.41−3.69 m^2/g, respectively, and the $S_{OM\text{-}non}$ are greater than the $S_{IM\text{-}non}$ for the samples with TOC content >4.65% (Table 4 and Figure 9c and d). The $V_{OM\text{-}mic}$ and $V_{IM\text{-}mic}$ of the YQ1 samples are 0.0018−0.0055 cm^3/g and 0.0007−0.0020 cm^3/g, respectively, and the $V_{OM\text{-}mic}$ of this set of shale samples is greater than its $V_{IM\text{-}mic}$. The $S_{OM\text{-}non}$ and $S_{IM\text{-}non}$ of the YQ1 samples are 1.40−4.34 m^2/g and 1.84−3.04 m^2/g, respectively, and the $S_{OM\text{-}non}$ is greater than the $S_{IM\text{-}non}$ for the samples with TOC content >2.89% (Table 4 and Figure 9c and d). It should be pointed out that the calculated organic-hosted and inorganic-hosted porosity or pore structure values only cover the open pores of the shales, excluding the closed organic-hosted and inorganic-hosted pores in the shale matrix.

The evolutions of organic-hosted pores are mainly controlled by the kerogen degradation and hydrocarbon expulsion. The volume shrinkage of kerogen provided significant pore spaces for the generated oils, and organic-hosted pores formed as the oils were expulsed from the shale matrix or cracked into gas.[63−65] The evolutions of inorganic-hosted pores are mainly controlled by the compaction of overlying strata, the filling of hydrocarbons, and the transformation of clay minerals during thermal evolution stages.[66,67] Therefore, shale porosity and pore structures are influenced by several factors, mainly including the organic and inorganic composition and content, organic matter thermal maturities, as well as mineral diagenesis levels.[66−69] For overmature shales, although the porosity and pore structure are mainly controlled by their TOC content,[14] they could be altered with further increasing maturity.[67] According to a thermal simulation experiment carried out by Chen and Xiao,[70] when the maturity of a shale exceeds the dry gas window (approximately R_o = 3.5%), the volume and surface

DOI: 10.1021/acs.energyfuels.8b03011
Energy Fuels 2018, 32, 11452−11466

area of the micropores and the mesopore surface area would decrease as the maturity increases because of the conversion of micropores into mesopores and the pore size expansion of the mesopores. The Lower Cambrian shales generally have lower porosities compared with the Lower Silurian shales in southern China,[12,13,23] which is attributed to a more intense diagenesis and compaction of the Lower Cambrian shales caused by a deeper burial or a higher maturity.[71] Given a certain TOC content, the total porosity, organic-hosted porosity, and pore structure parameters of the FY1 shales are lower than those of the YQ1 shales (Table 4), which is probably due to the same reason as mentioned above: a higher maturity and a stronger diagenesis of the FY1 samples caused by a deeper burial (Table 1).

3.4. TOC Content Control of the Water in Overmature Shales. Theoretically, the C_{IW} and C_{EIW} of overmature shales are mainly controlled by their hydrophilic pore volumes and surface areas under a certain geological condition and will increase with increasing these pore structure parameters. However, the S_{EW} of these shales mainly depends on the relative ratio of their hydrophilic to hydrophobic pores, i.e., the ratio of the hydrophilic to hydrophobic pore volumes and/or hydrophilic to hydrophobic pore surface areas, and will increase with the increase of these ratios. The organic matter in shales is conventionally considered hydrophobic, and the organic-hosted pores rarely hold water due to the drainage of hydrocarbon generation and expulsion; in contrast, the inorganic matter (mainly clay minerals) in shales is more hydrophilic due to its higher values of cation-exchange capacity and surface charge density,[52,72,73] and thus the water in shales is mainly stored in their inorganic-hosted pores.[29,33,42,74,75] However, recent studies show that some organic-hosted pores in shales can also hold water molecules.[38,76−80] The generally accepted mechanism is that the surfaces of the organic-hosted pores have some hydrophilic oxygen-containing functional groups, which could capture water through hydrogen bonding with water molecules.[38,62,81−86] Alternatively, several studies indicate that porous organic matter, such as porous carbon and graphite, even without oxygen-containing functional groups, also presents a mild hydrophilia and holds water through the interaction force existing between nanopore walls and water molecules;[32,79,87] the smaller the pore size of an organic-hosted nanopore, the stronger its hydrophilic capacity.[34] For the organic matter in overmature shales, the oxygen-containing functional groups may have degraded because of their aromatization, but the widely developed organic-hosted nanopores, especially micropores and mesopores,[14,67,88] provide more storage space for water, although the hydrophilia of these nanopores is weaker compared to their associated inorganic-hosted nanopores. Figure 10 shows that the P_{OM}, $V_{OM\text{-}mic}$, and $S_{OM\text{-}non}$ of both the FY1 and YQ1 samples have obvious positive relationships with the C_{IW} and C_{EIW}, and the coefficients (R^2) are 0.72−0.97 and 0.89−0.97, respectively, further indicating that the organic-hosted pores of these overmature shales could hold water. For a set of the studied shales, the shales with higher TOC contents have more nanopore spaces for storing water and thus have a higher C_{IW} and C_{EIW}.

Though water can be stored in the two types of shale pores, the organic-hosted pores are relatively hydrophobic compared with the inorganic-hosted pores. Figure 3a and Figure 11 present linear positive relationships of the TOC content with the C_{IW} and C_{EIW} of the FY1 and YQ1 samples, indicating the controls of the TOC content on the two parameters. Combining Figure 3a and Figure 11, the water equilibrium saturation of the organic-hosted pores (S_{OW}) and inorganic-hosted pores (S_{IW}) can be deduced for the two sets of shales. The slopes of the regression lines in Figure 3a and Figure 11 represent the average water content ($C_{IW\text{-}OM}$) and the average equilibrium irreducible water content ($C_{EIW\text{-}OM}$) held by the organic-hosted pores of the samples, respectively, and the S_{OW} can be estimated by the ratio of $C_{IW\text{-}OM}/C_{EIW\text{-}OM}$. The $C_{IW\text{-}OM}$ of the FY1 and YQ1 shales is 0.16 mg/g and 0.35 mg/g, respectively; the $C_{EIW\text{-}OM}$ of the FY1 and YQ1 shales is 0.81 mg/g and 1.39 mg/g, respectively (Figure 3a and Figure 11); and thus the ratios of $C_{IW\text{-}OM}/C_{EIW\text{-}OM}$ (i.e., the S_{OW}) are 19.75% for the FY1 samples and 25.18% for the YQ1 samples. The intercepts of the regression lines in Figure 3a and Figure 11 represent the average water content ($C_{IW\text{-}IM}$) and the average equilibrium irreducible water content ($C_{EIW\text{-}IM}$) held by the inorganic-hosted pores of the samples, respectively, and the ratio of $C_{IW\text{-}IM}/C_{EIW\text{-}IM}$ can be considered as the average water equilibrium saturation of the inorganic-hosted pores (S_{IW}). The $C_{IW\text{-}IM}$ of the FY1 and YQ1 shales is 3.90 mg/g and 3.25 mg/g, respectively, and the $C_{EIW\text{-}IM}$ of the FY1 and YQ1 shales is 8.65 mg/g and 6.33 mg/g, respectively (Figure 3a and Figure 11); thus, the ratios of $C_{IW\text{-}IM}/C_{EIW\text{-}IM}$ (i.e., the S_{IW}) are 45.09% for the FY1 samples and 51.34% for the YQ1 samples. According to these data, the S_{OW} of the two sets of shales is much lower than their S_{IW}, and the S_{IW}/S_{OW} ratio is 2.28 for the FY1 samples and 2.04 for the YQ1 samples, indicating that the inorganic-hosted pores of these overmature shales are more hydrophilic compared with their organic-hosted pores. It was reported that the hydrophilic capacity of inorganic-hosted pores in high-rank coals from the Bowen Basin, Australia, is 2.3−2.8 times larger than that of their organic-hosted pores,[89] which is similar with the overmature shales in the present study.

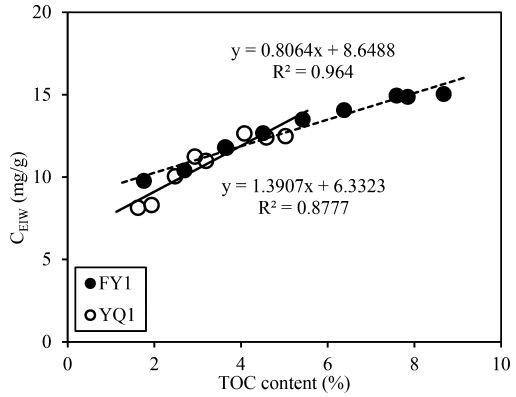

Figure 11. Correlations of the TOC content of the studied shale samples with their equilibrium irreducible water content (C_{EIW}). Data are presented in Table 1 and Table 2 and cited from ref 49.

Since the organic-hosted and inorganic-hosted pores of these overmature shales present different hydrophilic capacities, their bulk water wettability could be approximately characterized by the ratios of inorganic-hosted porosity/organic-hosted porosity (P_{IM}/P_{OM}), inorganic-hosted micropore volume/organic-hosted micropore volume ($V_{IM\text{-}mic}/V_{OM\text{-}mic}$), and inorganic-hosted nonmicropore surface area/organic-hosted nonmicropore surface area ($S_{IM\text{-}non}/S_{OM\text{-}non}$) (Table 4). These ratios show significant positive correlations with the TOC content (Figure 12) and significant negative correlations with the S_{EW} (Figure 13) for the two sets of overmature shale samples. Therefore, these shales become less hydrophilic with increasing TOC contents, which accounts for the associated decrease of the S_{EW}.

DOI: 10.1021/acs.energyfuels.8b03011
Energy Fuels 2018, 32, 11452−11466

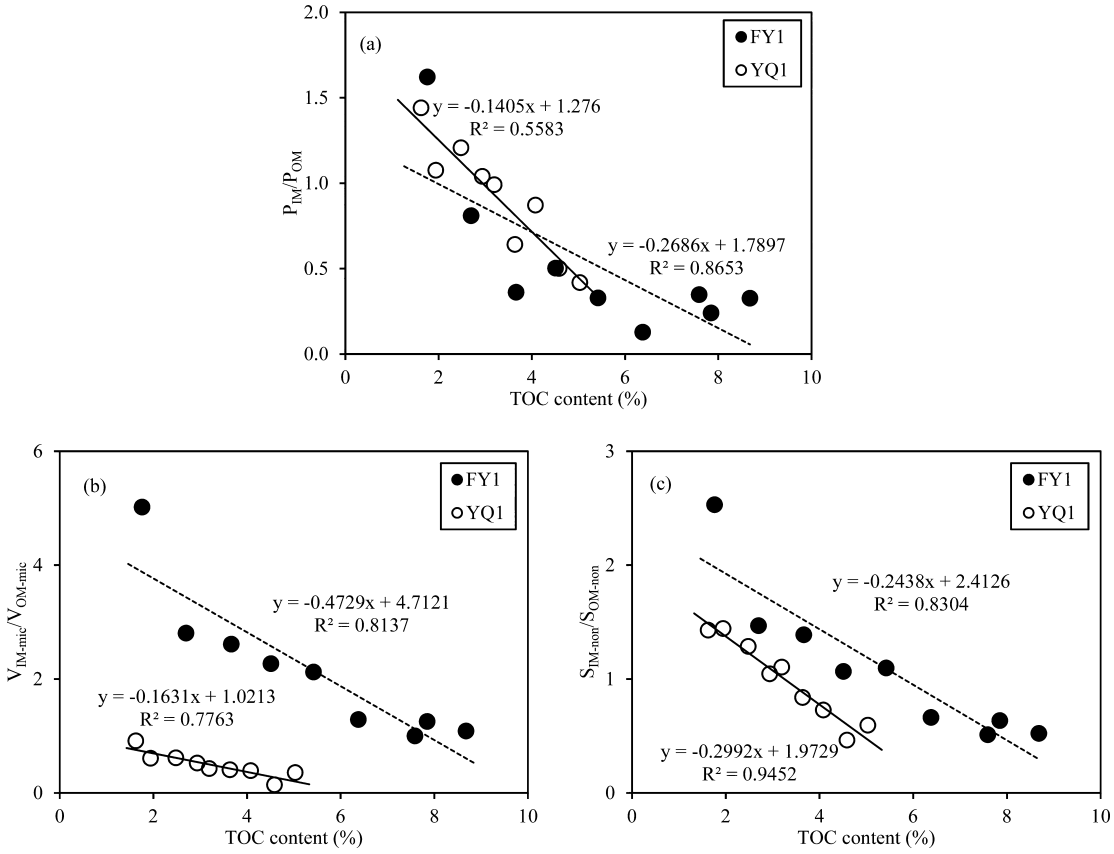

Figure 12. Correlations of the TOC content with the ratios of inorganic-hosted porosity/organic-hosted porosity (P_{IM}/P_{OM}) (a), inorganic-hosted micropore volume/organic-hosted micropore volume ($V_{IM\text{-}mic}/V_{OM\text{-}mic}$) (b), and inorganic-hosted nonmicropore surface area/organic-hosted nonmicropore surface area ($S_{IM\text{-}non}/S_{OM\text{-}non}$) (c) of the studied shale samples.

3.5. Implications of Water in Overmature Shales. Shale strata are deposited in a subaqueous environment, and thus they are saturated with water during sedimentary stages. During early diagenesis, the connate water gradually drains away from the shale matrix by compactions of overlying strata with increasing burial depth.[90] During the stages of petroleum generation and expulsion, this water is further reduced, mainly due to the displacement drainage of liquid hydrocarbons and the flow-through drying of gaseous hydrocarbons.[20,24−26] It has been reported that the water content of shales decreases with increasing thermal evolution, and the higher the maturity of shales, the lower their water content.[18] This correlation was also observed in coal samples, whose moisture content decreases with increasing coal ranks.[82] The organic-rich FY1 and YQ1 shale samples, whose original kerogen is type I or II_a, have experienced a burial depth of 7000−8000 m and 6000−7000 m,[8,9] reaching the end and late stage of dry gas generation, respectively.[5] The strong diagenesis, very high maturity, and exhaustive petroleum generation and expulsion are the reasons for their low water content and the subirreducible water-equilibrated state.

The Lower Cambrian and Lower Silurian shales, which widely developed in the Upper Yangtze Region of southern China, have equivalent vitrinite reflectance (ER_O) values of 3.0−4.5% and 2.5−3.5%, TOC contents of 2−8% and 2−5%, and total clay contents of 20−30% and 30−40%, respectively.[7,8,23] The Lower Paleozoic overmature shales and the FY1 and YQ1 shales are similar in geochemical parameters (Table 1), and thus, the water characteristics in the Lower Paleozoic overmature shales could be partially determined by those of the two sets of shales. The C_{IW} of five Longmaxi Formation shale samples, derived from the Jiaoye 4 well in the Sichuan Basin, was measured to be 2.73−6.14 mg/g by TRA (Tight Rock Analysis) technology[21] and was consistent with that of the YQ1 samples in the present study (Table 2). Since the free water in a shale reservoir only occurs after it has been saturated by the irreducible water with a content approximating the C_{EIW},[34,39] it may be further deduced that the Lower Paleozoic overmature shale gas reservoirs, which are in a subirreducible water-equilibrated state, are almost without connate free water, unless the shale reservoirs were damaged by tectonic movements and subsequently injected with sedimentary water.

A low water content in shale reservoir is beneficial to the storage of shale gas resources since the water in the shale reservoir occupies a certain amount of its pore spaces, which would result in the reduction of both the free and adsorbed gas content.[4,30,41,47] However, the low water content is harmful to the production of shale gas because the fracturing water could spontaneously imbibe into the shale pore system and block its connectivity.[20,36,91] Meanwhile, a subirreducible water-equilibrated state of shale reservoirs leads to a low flow-back rate of the fracturing water and thus wastes water resources;[92,93] this is a significant disadvantage for the shale gas development in the Upper Yangtze Region of southern China where water resources are generally lacking.[10] Therefore, both beneficial and harmful aspects of a low water content and equilibrium saturation in overmature shales should be considered when evaluating, exploring, and developing the shale gas in southern China.

DOI: 10.1021/acs.energyfuels.8b03011
Energy Fuels 2018, 32, 11452−11466

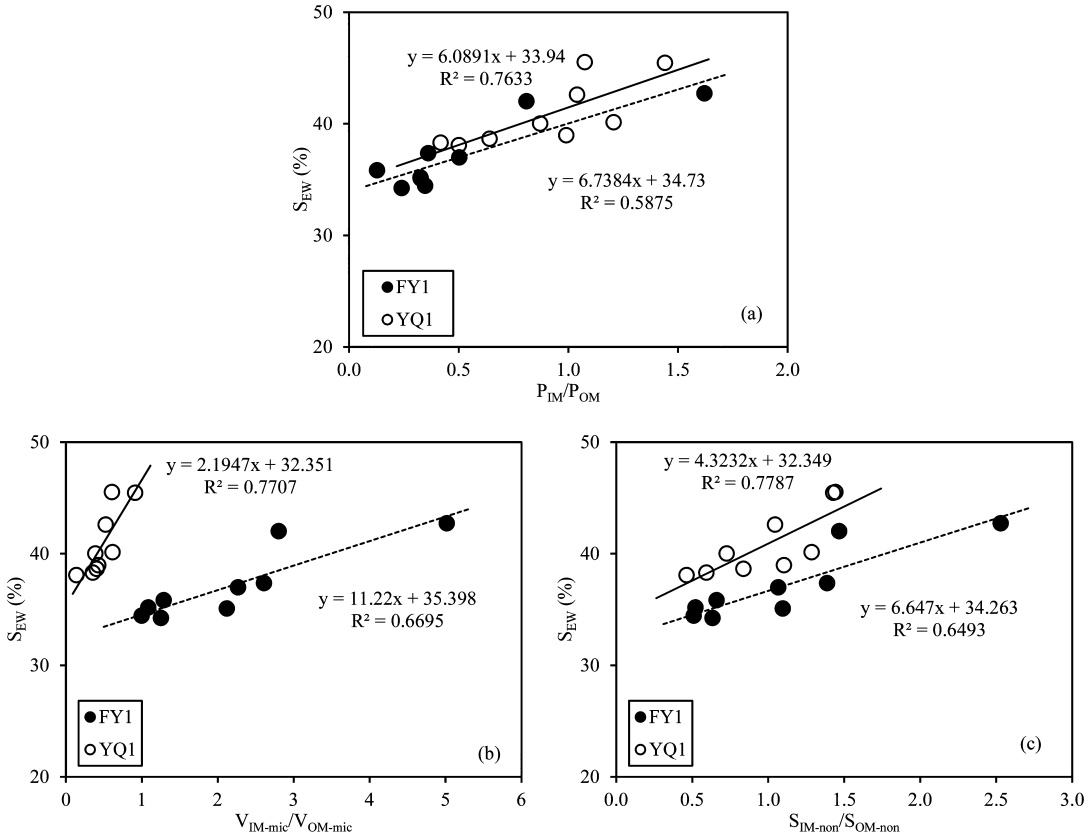

Figure 13. Correlations of the water equilibrium saturation (S_{EW}) with the ratios of inorganic-hosted porosity/organic-hosted porosity (P_{IM}/P_{OM}) (a), inorganic-hosted micropore volume/organic-hosted micropore volume ($V_{IM\text{-}mic}/V_{OM\text{-}mic}$) (b), and inorganic-hosted nonmicropore surface area/organic-hosted nonmicropore surface area ($S_{IM\text{-}non}/S_{OM\text{-}non}$) (c) of the studied shale samples.

4. CONCLUSIONS

In the present study, the water content (C_{IW}, i.e., the irreducible water content) and equilibrium saturation (S_{EW}, the percentage of C_{IW} in C_{EIW}, here C_{EIW} is the equilibrium irreducible water content at a relative humidity of 96−97% and 30 °C), as well as their influencing factors of two sets of as-received overmature organic-rich shale samples, respectively, derived from the Lower Cambrian Niutitang Formation of Fengye 1 well (FY1) and the Lower Silurian Longmaxi Formation of Youqian 1 well (YQ1) in the Upper Yangtze Region of southern China, were investigated. Several conclusions are summarized here:

(1) The C_{IW} of the FY1 and YQ1 samples is 4.17−5.29 mg/g and 3.70−5.06 mg/g, respectively. The S_{EW} of the FY1 and YQ1 shales is 34.23−42.72% and 38.07−45.51%, respectively, indicating both sets of shales are in a subirreducible water-equilibrated state.

(2) The C_{IW} and C_{EIW} of overmature shales are positively correlated with their TOC content, total porosity, surface area, and pore volume of both the micropores and nonmicropores; however, the S_{EW} of these shales is negatively correlated with these parameters.

(3) Water can store in the organic-hosted pores of overmature shales as well as in the inorganic-hosted pores, and the water equilibrium saturation of the inorganic-hosted pores (S_{IW}) is greater than that of the organic-hosted pores (S_{OW}). The S_{IW}/S_{OW} ratio of the FY1 and YQ1 overmature shales is 2.28 and 2.04, respectively.

(4) The TOC content controls the porosity and pore structures of overmature shales; additionally, these parameters control the bulk water wettability and water-storage spaces of these shales. Thus, under a certain geological condition, the TOC content may be the dominating factor that affects the C_{IW}, C_{EIW}, and S_{EW} of a set of overmature shales.

AUTHOR INFORMATION

Corresponding Author

*E-mail: xmxiao@gig.ac.cn.

ORCID

Peng Cheng: 0000-0002-3156-5712

Notes

The authors declare no competing financial interest.

ACKNOWLEDGMENTS

We are indebted to three anonymous reviewers for their insightful comments and suggestions that have much improved the manuscript. This study was supported by the National Natural Science Foundation of China (41402116, 41621062), National Science and Technology Major Project of China (2017ZX05008-002-004), the Special Program of Chinese Academy of Science (XDB10040300, XDA14010104), and The 973 Program of China (2012CB214705). Associate editor Minghou Xu is also acknowledged for his patient editorial work. This is contribution No.IS-2600 from GIGCAS.

NOMENCLATURE

C_{IW} = water content
C_{EIW} = equilibrium irreducible water content

DOI: 10.1021/acs.energyfuels.8b03011
Energy Fuels 2018, 32, 11452−11466

S_{EW} = water equilibrium saturation
FY1 = Fengye 1 well
YQ1 = Youqian 1 well
S_{OW} = water equilibrium saturation of the organic-hosted pore
S_{IW} = water equilibrium saturation of the inorganic-hosted pore
TOC = total organic carbon
BR_O = pyrobitumen reflectance value
ER_O = equivalent vitrinite reflectance value
m_{AR} = mass of as-received shale sample
m_{Dry} = mass of dry shale sample
ρ_s = the skeletal density
ρ_B = the bulk density
Φ = the total porosity
V_{mic} = micropore volume
S_{mic} = micropore surface area
$S_{n\text{-}mic}$ = nonmicropore surface area
$V_{n\text{-}mic}$ = nonmicropore volume
W_{OM} = average organic-hosted porosity of per 1% of TOC content
P_{OM} = organic-hosted porosity
P_{IM} = inorganic-hosted porosity
$S_{OM\text{-}non}$ = organic-hosted nonmicropore surface area
$S_{IM\text{-}non}$ = inorganic-hosted nonmicropore surface area
$V_{OM\text{-}mic}$ = organic-hosted micropore volume
$C_{IW\text{-}OM}$ = average water content in organic-hosted pore
$V_{IM\text{-}mic}$ = inorganic-hosted micropore volume
$C_{EIW\text{-}OM}$ = average equilibrium irreducible water content held by organic-hosted pore
$C_{IW\text{-}IM}$ = average water content in inorganic-hosted pore
TRA = tight rock analysis
$C_{EIW\text{-}IM}$ = average equilibrium irreducible water content held by inorganic-hosted pore

REFERENCES

(1) Ross, D. J. K.; Bustin, R. M. Characterizing the shale gas resource potential of Devonian-Mississippian strata in the Western Canada Sedimentary Basin: application of an integrated formation evaluation. *AAPG Bull.* **2008**, *92*, 87−125.

(2) Ambrose, R. J.; Hartman, R. C.; Campos, M. D.; Akkutlu, I. Y.; Sondergeld, C. H. New pore-scale considerations for shale gas in place calculations. *Society of Petroleum Engineers* **2010**, *SPE-131772-MS*, 1−17.

(3) Handwerger, D. A.; Suarez-Rivera, R.; Vaughn, K. I.; Keller, J. F. Improved petrophysical core measurements on tight shale reservoirs using retort and crushed samples. *Society of Petroleum Engineers* **2011**, *SPE-147456-MS*, 1−20.

(4) Gasparik, M.; Bertier, P.; Gensterblum, Y.; Ghanizadeh, A.; Krooss, B. M.; Littke, R. Geological controls on the methane storage capacity in organic-rich shales. *Int. J. Coal Geol.* **2014**, *123*, 34−51.

(5) Cheng, P.; Xiao, X. M. Gas content of organic-rich shales with very high maturities. *J. China Coal Soc.* **2013**, *38* (5), 737−741 (In Chinese with English abstract) .

(6) Zou, C. N.; Dong, D. Z.; Wang, Y. M.; Li, X. J.; Huang, J. L.; Wang, S. F.; Guan, Q. Z.; Zhang, C. C.; Wang, H. Y.; Liu, H. L.; Bai, W. H.; Liang, F.; Lin, W.; Zhao, Q.; Liu, D. X.; Yang, Z.; Liang, P. P.; Sun, S. S.; Qiu, Z. Shale gas in China: characteristics, challenges and prospects (II). *Petrol. Explor. Dev.* **2016**, *43* (2), 182−196.

(7) Zhang, J. C.; Jiang, S. L.; Tang, X.; Zhang, P. X.; Tang, Y.; Jin, T. Y. Accumulation types and resources characteristics of shale gas in China. *Nat. Gas Ind.* **2009**, *29*, 109−114 (In Chinese with English abstract) .

(8) Dong, D. Z.; Gao, S. K.; Huang, J. L.; Guan, Q. Z.; Wang, S. F.; Wang, Y. M. A discussion on the shale gas exploration and development prospect in the Sichuan Basin. *Nat. Gas Ind.* **2014**, *34*, 1−13 (In Chinese with English abstract) .

(9) Liu, S. G.; Deng, B.; Zhong, Y.; Ran, B.; Yong, Z. Q.; Sun, W.; Yang, D.; Jiang, L.; Ye, Y. H. Unique geological features of burial and superimposition of Lower Paleozoic shale gas across the Sichuan Basin and its periphery. *Earth Sci. Front.* **2016**, *23*, 11−28 (In Chinese with English abstract) .

(10) Dong, D. Z.; Wang, Y. M.; Li, X. J.; Zou, C. N.; Guan, Q. Z.; Zhang, C. C.; Huang, J. L.; Wang, S. F.; Wang, H. Y.; Liu, H. L.; Bai, W. H.; Liang, F.; Ji, W.; Zhao, Q.; Liu, D. X.; Qiu, Z. Breakthrough and prospect of shale gas exploration and development in China. *Nat. Gas Ind.* **2016**, *3*, 12−26 (In Chinese with English abstract) .

(11) Ma, Y. S.; Cai, X. Y.; Zhao, P. R. China's shale gas exploration and development: Understanding and practice. *Petrol. Explor. Dev.* **2018**, *45* (4), 589−603.

(12) Tian, H.; Pan, L.; Xiao, X. M.; Wilkins, R. W. T.; Meng, Z. P.; Huang, B. J. A preliminary study on the pore characterization of Lower Silurian black shales in the Chuandong Thrust Fold Belt, southwestern China using low pressure N_2 adsorption and FE-SEM methods. *Mar. Pet. Geol.* **2013**, *48*, 8−19.

(13) Tian, H.; Pan, L.; Zhang, T. W.; Xiao, X. M.; Meng, Z. P.; Huang, B. J. Pore characterization of organic-rich Lower Cambrian shales in Qiannan Depression of Guizhou Province, Southwestern China. *Mar. Pet. Geol.* **2015**, *62*, 28−43.

(14) Hu, H. Y.; Hao, F.; Lin, J. F.; Lu, Y. C.; Ma, Y. Q.; Li, Q. Organic matter-hosted pore system in the Wufeng-Longmaxi (O_{3w}-S_{11}) shale, Jiaoshiba area, Eastern Sichuan Basin, China. *Int. J. Coal Geol.* **2017**, *173*, 40−50.

(15) Li, T. F.; Tian, H.; Xiao, X. M.; Cheng, P.; Zhou, Q.; Wei, Q. Geochemical characterization and methane adsorption capacity of overmature organic-rich Lower Cambrian shales in northeast Guizhou Region, southwest China. *Mar. Pet. Geol.* **2017**, *86*, 858−873.

(16) Yang, R.; Hao, F.; He, S.; He, C. C.; Guo, X. S.; Yi, J. Z.; Hu, H. Y.; Zhang, S. W.; Hu, Q. H. Experimental investigations on the geometry and connectivity of pore space in organic-rich Wufeng and Longmaxi shales. *Mar. Pet. Geol.* **2017**, *84*, 225−242.

(17) Powers, M. C. Fluid release mechanisms in compacting marine mudrocks and their importance in oil exploration. *AAPG Bull.* **1967**, *51*, 1240−1254.

(18) Gensterblum, Y.; Amin Ghanizadeh, A.; Cuss, R. J.; Amann-Hildenbrand, A.; Krooss, B. M.; Clarkson, C. R.; Harrington, J. F.; Zoback, M. D. Gas storage capacity and transport in shale gas reservoirs - a review. Part A: Transport processes. *J. Unconv. Oil Gas Resour.* **2015**, *12*, 87−122.

(19) Liu, H. L.; Wang, H. Y.; Fang, Z. H.; Guo, W.; Sun, S. S. The formation mechanism of over-pressure reservoir and target screening index of the marine shale in the South China. *Earth Sci. Front.* **2016**, *23*, 48−54 (In Chinese with English abstract) .

(20) Liu, H. L.; Wang, H. Y. Ultra-low water saturation characteristics and the identification of over-pressured play fairways of marine shales in south China. *Nat. Gas Ind.* **2013**, *33* (7), 140−144 (In Chinese with English abstract) .

(21) Wei, Z. H.; Wei, X. F. Comparison of gas-bearing property between different pore types of shales: A case from the Upper Ordovician Wufeng and Longmaxi formations in the Jiaoshiba area, Sichuan, China. *Nat. Gas Ind.* **2014**, *34* (6), 37−41 (In Chinese with English abstract) .

(22) Zhang, T. W.; Geoffrey, S. E.; Stephen, C. R.; Kitty, M.; Yang, R. S. Effect of organic matter type and thermal maturity on methane adsorption in shale gas system. *Org. Geochem.* **2012**, *47*, 120−131.

(23) Xiao, X. M.; Wang, M. L.; Wei, Q.; Tian, H.; Pan, L.; Li, T. F. Evaluation of Lower Paleozoic shale with shale gas prospect in south China. *Nat. Gas Geosci.* **2015**, *26* (8), 1433−1445 (In Chinese with English abstract) .

(24) Wardlaw, N. C.; McKellar, M. Wettability and connate water saturation in hydrocarbon reservoirs with bitumen deposits. *J. Pet. Sci. Eng.* **1998**, *20*, 141−146.

DOI: 10.1021/acs.energyfuels.8b03011
Energy Fuels 2018, 32, 11452−11466

(25) Mahadevan, J.; Sharma, M.; Yortsos, Y. C. Water removal from porous media by gas injection: experiments and simulation. *Transp. Porous Media* **2007**, *66*, 287−309.
(26) Fang, Z. H.; Huang, Z. L.; Wang, Q. Z.; Deng, D. W.; Liu, H. L. Cause and significance of the ultra-low water saturation in gas-riched shale reservoir. *Nat. Gas Geosci.* **2014**, *25*, 471−475 (In Chinese with English abstract) .
(27) Humphreys, N. V. The material balance equation for a gas condensate reservoir with significant water vaporization. *Society of Petroleum Engineers* **1991**, *SPE 21514*, 1−8.
(28) Borysenko, A.; Clennell, B.; Sedev, R.; Burgar, I.; Ralston, J.; Raven, M.; Dewhurst, D.; Liu, K. Y. Experimental investigations of the wettability of clays and shales. *J. Geophys. Res.* **2009**, *114*, 1−11.
(29) Passey, Q. R.; Bohacs, K. M.; Esch, W. L.; Klimentidis, R.; Sinha, S. From oil-prone source rock to gas-producing shale reservoir - geologic and petrophysical characterization of unconventional shale-gas reservoirs. *Society of Petroleum Engineers* **2010**, *SPE-131350-MS*, 1−29.
(30) Odusina, E.; Sondergeld, D. C.; Rai, D. C. An NMR study on shale wettability. *Society of Petroleum Engineers* **2011**, *SPE-147371-MS*, 1−15.
(31) Wen, H.; Chen, M.; Jin, Y.; Zhang, Y. Y.; Ge, W. F.; Du, J. L.; Zeng, C. Water activity characteristics of deep brittle shale from Southwest China. *Appl. Clay Sci.* **2015**, *108*, 165−172.
(32) Liu, J. C.; Monson, P. A. Does water condense in carbon pores? *Langmuir* **2005**, *21*, 10219−10225.
(33) Li, J.; Li, X. F.; Wang, X. Z.; Li, Y. Y.; Wu, K. L.; Shi, J. T.; Yang, L.; Feng, D.; Zhang, T.; Yu, P. L. Water distribution characteristic and effect on methane adsorption capacity in shale clay. *Int. J. Coal Geol.* **2016**, *159*, 135−154.
(34) Wu, K. L.; Chen, Z. X.; Li, J.; Li, X. F.; Xu, J. Z.; Dong, X. H. Wettability effect on nanoconfined water flow. *Proc. Natl. Acad. Sci. U. S. A.* **2017**, *114*, 3358−3363.
(35) Keijzer, T. J.; Loch, J. P. G. Chemical osmosis in compacted dredging sludge. *Soil Sci. Soc. Am. J.* **2001**, *65*, 1045−1055.
(36) Dehghanpour, H.; Lan, Q.; Saeed, Y.; Fei, H.; Qi, Z. Spontaneous imbibition of brine and oil in gas shales: Effect of water adsorption and resulting microfractures. *Energy Fuels* **2013**, *27*, 3039−3049.
(37) Fakcharoenphol, P.; Kazemi, H.; Wu, Y. S.; Kurtoglu, B.; Charoenwongsa, S. The effect of osmotic pressure on improve oil recovery from fractured shale formations. *Society of Petroleum Engineers* **2014**, *SPE-168998-MS*, 1−12.
(38) Hu, Y. N.; Devegowda, D.; Sigal, R. A microscopic characterization of wettability in shale kerogen with varying maturity levels. *J. Nat. Gas Sci. Eng.* **2016**, *33*, 1078−1086.
(39) Bennion, D. B.; Thomas, F. B. Formation damage issues impacting the productivity of low permeability, low initial water saturation gas producing formations. *J. Energy Resour. Technol.* **2005**, *127* (3), 240−247.
(40) Bowker, K. A. Barnett shale gas production, Fort Worth Basin: Issues and discussion. *AAPG Bull.* **2007**, *91*, 523−533.
(41) Bustin, R. M.; Bustin, A. M. M.; Cui, X.; Ross, D. J. K.; Murthy Pathi, V. S. Impact of shale properties on pore structure and storage characteristics. *Society of Petroleum Engineers* **2008**, *SPE-119892-MS*, 1−28.
(42) Korb, J. P.; Nicot, B.; Louis-Joseph, A.; Bubici, S.; Ferrante, G. Dynamics and wettability of oil and water in oil shales. *J. Phys. Chem. C* **2014**, *118*, 23212−23218.
(43) Sondergeld, C. H.; Newsham, K. E.; Comisky, J. T.; Rice, M. C.; Rai, C. S. Petrophysical considerations in evaluating and producing shale gas resources. *Society of Petroleum Engineers* **2010**, *SPE-131768-MS*, 1−34.
(44) Ramirez, T. R.; Klein, J. D.; Bonnie, R.; Howard, J. J. Comparative study of formation evaluation methods for unconventional shale gas reservoirs: application to the Haynesville Shale (Texas). *Society of Petroleum Engineers* **2011**, 1−31.
(45) Zhang, B. Y.; Xu, J. L. Methods for the evaluation of water saturation considering TOC in shale reservoirs. *J. Nat. Gas Sci. Eng.* **2016**, *36*, 800−810.
(46) Bustin, R. M.; Clarkson, C. R. Geological controls on coalbed methane reservoir capacity and gas content. *Int. J. Coal Geol.* **1998**, *38*, 3−26.
(47) Hartman, R. C.; Lasswell, P.; Bhatta, N. *Recent advances in the analytical methods used for shale gas reservoir gas-in-place assessment*; AAPG Annual Convention: San Antonio, TX, 2008, April 20 − 23.
(48) Gensterblum, Y.; Merkel, A.; Busch, A.; Krooss, B. M. High-pressure CH_4 and CO_2 sorption isotherms as a function of coal thermal maturity and the influence of moisture. *Int. J. Coal Geol.* **2013**, *118*, 45−57.
(49) Cheng, P.; Tian, H.; Xiao, X. M.; Gai, H. F.; Li, T. F.; Wang, X. Water distribution in overmature organic-rich shales: Implications from water adsorption experiments. *Energy Fuels* **2017**, *31*, 13120−13132.
(50) Schoenherr, J.; Littke, R.; Urai, J. L.; Kukla, P. A.; Rawahi, Z. Polyphase thermal evolution in the Infra-Cambrian Ara group (South Oman salt basin) as deduced by maturity of solid reservoir bitumen. *Org. Geochem.* **2007**, *38*, 1293−1318.
(51) Boţan, A.; Rotenberg, B.; Marry, V.; Turq, P.; Noetinger, B. Hydrodynamics in clay nanopores. *J. Phys. Chem. C* **2011**, *115* (32), 16109−16115.
(52) Li, J.; Li, X. F.; Wu, K. L.; Feng, D.; Zhang, T.; Zhang, Y. F. Thickness and stability of water film confined inside nanoslits and nanocapillaries of shale and clay. *Int. J. Coal Geol.* **2017**, *179*, 253−268.
(53) Chalmers, G. R.; Bustin, R. M.; Power, I. M. Characterization of gas shale pore systems by porosimetry, pycnometry, surface area, and field emission scanning electron microscopy/transmission electron microscopy image analyses: examples from the Barnett, Woodford, Haynesville, Marcellus, and Doig units. *AAPG Bull.* **2012**, *96*, 1099−1119.
(54) Rouquerol, J.; Avnir, D.; Fairbridge, C. W.; Everett, D. H.; Haynes, J. H.; Pernicone, N.; Ramsay, J. D. F.; Sing, K. S. W.; Unger, K. Physical chemistry division commission on colloid and surface chemistry, subcommittee on characterization of porous solids: recommendations for the characterization of porous solids. *Pure Appl. Chem.* **1994**, *68*, 1739−1758.
(55) Clarkson, C. R.; Bustin, R. M. The effect of pore structure and gas pressure upon the transport properties of coal: a laboratory and modeling study 1. Isotherms and pore volume distributions. *Fuel* **1999**, *78*, 1333−1344.
(56) Clarkson, C. R.; Bustin, R. M. Binary gas adsorption/desorption isotherms: effect of moisture and coal composition upon carbon dioxide selectivity over methane. *Int. J. Coal Geol.* **2000**, *42*, 241−271.
(57) Ross, D. J. K.; Bustin, R. M. The importance of shale composition and pore structure upon gas storage potential of shale gas reservoirs. *Mar. Pet. Geol.* **2009**, *26*, 916−927.
(58) Pan, L.; Xiao, X. M.; Tian, H.; Zhou, Q.; Chen, J.; Li, T. F.; Wei, Q. A preliminary study on the characterization and controlling factors of porosity and pore structure of the Permian shales in Lower Yangtze Region, Eastern China. *Int. J. Coal Geol.* **2015**, *146*, 68−78.
(59) Dubinin, M. M. Fundamentals of the theory of adsorption in micropores of carbon adsorbents: characteristics of their adsorption properties and microporous structures. *Carbon* **1989**, *27* (3), 457−467.
(60) Brunauer, S.; Emmett, P. H.; Teller, E. Adsorption of gases in multimolecular layers. *J. Am. Chem. Soc.* **1938**, *60* (2), 309−319.
(61) Newsham, K. E.; Rushing, J. A.; Lasswell, P. M. Use of vapor desorption data to characterize high vapillary pressures in a basin-centered gas accumulation with ultra-low connate water saturations. *Society of Petroleum Engineers* **2003**, *SPE-84596-MS*, 1−9.
(62) Charrière, D.; Philippe Behra, P. Water sorption on coals. *J. Colloid Interface Sci.* **2010**, *344*, 460−467.
(63) Bernard, S.; Wirth, R.; Schreiber, A.; Schulz, H. M.; Horsfield, B. Formation of nanoporous pyrobitumen residues during maturation of the Barnett Shale (Fort Worth Basin). *Int. J. Coal Geol.* **2012**, *103*, 3−11.
(64) Mastalerz, M.; Schimmelmann, A.; Drobniak, A.; Chen, Y. Y. Porosity of Devonian and Mississippian New Albany Shale across a maturation gradient: Insights from organic petrology, gas adsorption, and mercury intrusion. *AAPG Bull.* **2013**, *97*, 1621−1643.

DOI: 10.1021/acs.energyfuels.8b03011
Energy Fuels 2018, 32, 11452−11466

(65) Valenza, J. J., II; Drenzek, N.; Marques, F.; Pagels, M.; Mastalerz, M. Geochemical controls on shale microstructure. *Geology* **2013**, *41* (5), 611−614.
(66) Loucks, R. G.; Reed, R. M.; Ruppel, S. C.; Hammes, U. Spectrum of pore types and networks in mudrocks and a descriptive classification for matrix-related mudrock pores. *AAPG Bull.* **2012**, *96*, 1071−1098.
(67) Pommer, M.; Milliken, K. Pore types and pore-size distributions across thermal maturity, Eagle Ford Formation, southern Texas. *AAPG Bull.* **2015**, *99*, 1713−1744.
(68) Curtis, M. E.; Cardott, B. J.; Sondergeld, C. H.; Rai, C. S. Development of organic porosity in the Woodford Shale with increasing thermal maturity. *Int. J. Coal Geol.* **2012**, *103*, 26−31.
(69) Guo, H. J.; Jia, W. L.; Peng, P. A.; Zeng, J.; He, R. L. Evolution of organic matter and nanometer-scale pores in an artificially matured shale undergoing two distinct types of pyrolysis: A study of the Yanchang shale with type II kerogen. *Org. Geochem.* **2017**, *105*, 56−66.
(70) Chen, J.; Xiao, X. M. Evolution of nanoporosity in organic-rich shales during thermal maturation. *Fuel* **2014**, *129*, 173−181.
(71) Wang, F. Y.; Guan, J.; Feng, W. P.; Bao, L. Y. Evolution of overmature marine shale porosity and implication to the free gas volume. *Petrol. Explor. Dev.* **2013**, *40* (6), 819−824.
(72) Bertier, P.; Seemann, T.; Krooss, B. M.; Stanjek, H. Water vapour sorption on mudrocks. *Fifth EAGE Shale Workshop*; Catania, Italy, 2−4 May 2016, DOI: 10.3997/2214-4609.201600394.
(73) Seemann, T.; Bertier, P.; Krooss, B. M.; Stanjek, H. Water vapour sorption on mudrocks. *Geol. Soc. Spec. Publ.* **2017**, *454*, 201.
(74) Zolfaghari, A.; Dehghanpour, H.; Holyk, J. Water sorption behaviour of gas shales: I. Role of clays. *Int. J. Coal Geol.* **2017**, *179*, 130−138.
(75) Zolfaghari, A.; Dehghanpour, H.; Xu, M. X. Water sorption behaviour of gas shales: II. Pore size distribution. *Int. J. Coal Geol.* **2017**, *179*, 187−195.
(76) Chalmers, G. R.; Bustin, R. M. The organic matter distribution and methane capacity of the Lower Cretaceous strata of Northeastern British Columbia, Canada. *Int. J. Coal Geol.* **2007**, *70*, 223−239.
(77) László, K.; Czakkel, O.; Dobos, G.; Lodewyckx, P.; Rochas, C.; Geissler, E. Water vapour adsorption in highly porous carbons as seen by small and wide angle X-ray scattering. *Carbon* **2010**, *48*, 1038−1048.
(78) Kozbial, A.; Li, Z. T.; Sun, J. N.; Gong, X.; Zhou, F.; Wang, Y. J.; Xu, H. C.; Liu, H. T.; Li, L. Understanding the intrinsic water wettability of graphite. *Carbon* **2014**, *74*, 218−225.
(79) Wei, Y. Y.; Jia, C. Q. Intrinsic wettability of graphitic carbon. *Carbon* **2015**, *87*, 10−17.
(80) Gu, X.; Mildner, D. F. R.; Cole, D. R.; Rother, G.; Slingerland, R.; Brantley, S. L. Quantification of organic porosity and water accessibility in Marcellus shale using neutron scattering. *Energy Fuels* **2016**, *30*, 4438−4449.
(81) Bekyarova, E.; Hanzawa, Y.; Kaneko, K.; Silvestre-Albero, J.; Sepulveda-Excribano, A.; Rodriguez-Reinoso, F.; Kasuya, D.; Yudasaka, M.; Iijima, S. Cluster-mediated filling of water vapor in intratube and interstitial nanospaces of single-wall carbon nanohorns. *Chem. Phys. Lett.* **2002**, *366*, 463−468.
(82) McCutcheon, A. L.; Barton, W. A.; Wilson, M. A. Characterization of water adsorbed on bituminous coals. *Energy Fuels* **2003**, *17*, 107−112.
(83) Do, D. D.; Junpirom, S.; Do, H. D. A new adsorption-desorption model for water adsorption in activated carbon. *Carbon* **2009**, *47*, 1466−1473.
(84) Hu, Y. N.; Devegowda, D.; Striolo, A.; Van Phan, A. T.; Ho, T. A.; Civan, F. Microscopic dynamics of water and hydrocarbon in shale-kerogen pores of potentially mixed wettability. *Society of Petroleum Engineers* **2013**, *SPE-167234-MS*, 1−14.
(85) Bahadur, J.; Contescu, C. I.; Rai, D. K.; Gallego, N. C.; Melnichenko, Y. B. Clustering of water molecules in ultramicroporous carbon: In-situ small-angle neutron scattering. *Carbon* **2017**, *111*, 681−688.
(86) Mamontov, E.; Yue, Y.; Bahadur, J.; Guo, J.; Contescu, C. I.; Gallego, N. C.; Melnichenko, Y. B. Hydration level dependence of the microscopic dynamics of water adsorbed in ultramicroporous carbon. *Carbon* **2017**, *111*, 705−712.
(87) Striolo, A.; Naicker, P. K.; Chialvo, A. A.; Cummings, P. T.; Gubbins, K. E. Simulated water adsorption isotherms in hydrophilic and hydrophobic cylindrical nanopores. *Adsorption* **2005**, *11*, 397−401.
(88) Loucks, R. G.; Reed, R. M.; Ruppel, S. C.; Jarvie, D. M. Morphology, genesis, and distribution of nanometer-scale pores in siliceous mudstones of the Mississippian Barnett Shale. *J. Sediment. Res.* **2009**, *79*, 848−861.
(89) McCutcheon, A. L.; Barton, W. A. Contribution of mineral matter to water associated with bituminous coals. *Energy Fuels* **1999**, *13*, 160−165.
(90) van Sickel, W. A.; Kominz, M. A.; Miller, K. G.; Browning, J. V. Late Cretaceous and Cenozoic sea level estimates: Backstripping analysis of borehole data, onshore New Jersey. *Basin Research* **2004**, *16*, 451−465.
(91) Dehghanpour, H.; Zubair, H. A.; Chhabra, A.; Ullah, A. Liquid intake of organic shales. *Energy Fuels* **2012**, *26*, 5750−5758.
(92) Engelder, T.; Cathles, L. M.; Bryndzia, L. T. The fate of residual treatment water in gas shale. *J. Unconv. Oil Gas Resour.* **2014**, *7*, 33−48.
(93) Burnaman, M. D.; Xia, W. W.; Shelton, J. Shale gas play screening and evaluation criteria. *China Petrol. Explor.* **2009**, *3*, 51−64.

DOI: 10.1021/acs.energyfuels.8b03011
Energy Fuels 2018, 32, 11452−11466